

# A multisite photometric study of two unusual $\beta$ Cep stars: the magnetic V2052 Oph and the massive rapid rotator V986 Oph

G. Handler,<sup>1</sup> R. R. Shobbrook,<sup>2</sup> K. Uytterhoeven,<sup>3,4</sup> M. Briquet,<sup>5,6</sup> C. Neiner,<sup>7</sup>  
T. Tshenye,<sup>8</sup> B. Ngwato,<sup>8</sup> H. van Winckel,<sup>6</sup> E. Guggenberger,<sup>9</sup> G. Raskin,<sup>6</sup>  
E. Rodríguez,<sup>10</sup> A. Mazumdar,<sup>11</sup> C. Barban,<sup>7</sup> D. Lorenz,<sup>9</sup> B. Vandenbussche,<sup>6</sup>  
T. Şahin,<sup>12,13</sup> R. Medupe,<sup>8</sup> C. Aerts<sup>6</sup>

<sup>1</sup> Copernicus Astronomical Center, Bartycka 18, 00-716 Warsaw, Poland (gerald@camk.edu.pl)

<sup>2</sup> Research School of Astronomy and Astrophysics, Australian National University, Canberra, ACT, Australia

<sup>3</sup> Instituto de Astrofísica de Canarias (IAC), E-38200 La Laguna, Tenerife, Spain

<sup>4</sup> Departamento de Astrofísica, Universidad de La Laguna (ULL), E-38206 La Laguna, Tenerife, Spain

<sup>5</sup> Institut d'Astrophysique et de Géophysique, Université de Liège, Allée du 6 Août 17, Bât B5c, 4000, Liège, Belgium

<sup>6</sup> Instituut voor Sterrenkunde, K. U. Leuven, Celestijnenlaan 200D, B-3001 Leuven, Belgium

<sup>7</sup> LESIA, Observatoire de Paris, CNRS UMR 8109, UPMC, Université Paris Diderot; 5 place Jules Janssen, 92190 Meudon, France

<sup>8</sup> Department of Physics, University of the North-West, Private Bag X2046, Mmabatho 2735, South Africa

<sup>9</sup> Institut für Astronomie, Universität Wien, Türkenschanzstrasse 17, A-1180 Wien, Austria

<sup>10</sup> Instituto de Astrofísica de Andalucía, C.S.I.C., Apdo. 3004, 18080 Granada, Spain

<sup>11</sup> Homi Bhabha Centre for Science Education (TIFR), V. N. Purav Marg, Mumbai 400088, India

<sup>12</sup> Akdeniz University, Faculty of Science, Space Science and Technologies Department, 07058, Antalya, Turkey

<sup>13</sup> TUBITAK National Observatory, Akdeniz University Campus, 07058, Antalya, Turkey

Accepted 2005 July 17. Received 2005 August 13; in original form 2005 September 10

## ABSTRACT

We report a multisite photometric campaign for the  $\beta$  Cep stars V2052 Oph and V986 Oph. 670 hours of high-quality differential photoelectric Strömrgren, Johnson and Geneva time-series photometry were obtained with eight telescopes on five continents during 182 nights. Frequency analyses of the V2052 Oph data enabled the detection of three pulsation frequencies, the first harmonic of the strongest signal, and the rotation frequency with its first harmonic. Pulsational mode identification from analysing the colour amplitude ratios confirms the dominant mode as being radial, whereas the other two oscillations are most likely  $l = 4$ . Combining seismic constraints on the inclination of the rotation axis with published magnetic field analyses we conclude that the radial mode must be the fundamental. The rotational light modulation is in phase with published spectroscopic variability, and consistent with an oblique rotator for which both magnetic poles pass through the line of sight. The inclination of the rotation axis is  $54^\circ < i < 58^\circ$  and the magnetic obliquity  $58^\circ < \beta < 66^\circ$ . The possibility that V2052 Oph has a magnetically confined wind is discussed. The photometric amplitudes of the single oscillation of V986 Oph are most consistent with an  $l = 3$  mode, but this identification is uncertain. Additional intrinsic, apparently temporally incoherent, light variations of V986 Oph are reported. Different interpretations thereof cannot be distinguished at this point, but this kind of variability appears to be present in many OB stars. The prospects of obtaining asteroseismic information for more rapidly rotating  $\beta$  Cep stars, which appear to prefer modes of higher  $l$ , are briefly discussed.

**Key words:** stars: variables: other – stars: early-type – stars: oscillations – stars: individual: V2052 Oph, V986 Oph – stars: magnetic field – stars: rotation

## 1 INTRODUCTION

For over a century, the  $\beta$  Cep stars are known to be variable on time scales of hours (Frost 1902), but it took half a century longer to understand the nature of their variability, radial and nonradial pulsations (Ledoux 1951). Nowadays, about 300 members of this class of pulsating star are known (Stankov & Handler 2005, Pigulski & Pojmański 2008).

Because of the simultaneous presence of radial and nonradial oscillation modes in these stars, and their rather simple overall structure (basically a convective core and a radiative envelope), their potential as asteroseismic targets is evident. Asteroseismology is the inference of the interior structure of pulsating stars. This is accomplished by measuring their oscillation frequencies, comparing them with the eigenfrequencies of corresponding stellar models, and then fine-tuning those models to match the observed frequencies (see, e.g., Aerts et al. 2010, Handler 2012).

Besides the Sun, the  $\beta$  Cep stars were the first main sequence pulsators for which clear constraints on their inner structure could be obtained asteroseismically (for a heavily abbreviated literature, see Aerts et al. 2003, Pamyatnykh et al. 2004, Handler et al. 2009, Aerts et al. 2011). Results indicate that further increases in heavy-element opacities are needed, and some stars have been shown to rotate faster in their interior than on the outside.

These first successful studies were in most cases intentionally biased towards bright, slowly rotating stars. Slowly rotating  $\beta$  Cep stars driven by the  $\kappa$  mechanism tend to have higher pulsation amplitudes (Stankov & Handler 2005) and therefore offer better possibilities for mode identification. Obviously, effects of rotation on the observed frequencies of axisymmetric modes of oscillation are also smaller, and rotationally split m-mode patterns would not overlap in frequency. This way of approaching asteroseismology of  $\beta$  Cep stars proved to be sound. Therefore it appears reasonable to investigate targets that pose more difficult initial conditions, but that may also be more rewarding astrophysically.

V2052 Oph (HR 6684,  $V = 5.8$ , B2IV-V) was discovered as a  $\beta$  Cep pulsator by Jerzykiewicz (1972), and its dominant mode identified as radial (Heynderickx, Waelkens & Smeyers 1994, Cugier, Dziembowski & Pamyatnykh 1994). Neiner et al. (2003) carried out an extensive multiwavelength spectroscopic and spectropolarimetric study of V2052 Oph that revealed several interesting properties of this star. Besides the detection of a second, nonradial, pulsation mode, these authors could derive an accurate rotation period of  $3.638833 \pm 0.000003$  d. V2052 Oph also possesses a dipole magnetic field. Based on new data of superior quality, Neiner et al. (2012a) determined  $B_{\text{pol}} \approx 400G$ , that the magnetic field is likely off-centred, and that He patches are present close to the magnetic poles. Because of the presence of a radial pulsation mode (that allows the determination of the mean stellar density), and of the known rotation period that makes it spin about twice as fast as the most "rapidly" rotating seismically well studied  $\beta$  Cep star (12 Lac, Desmet et al. 2009), it was deemed worthwhile to devote a large observational effort to V2052 Oph. To this end, the present paper reports photometric results of a multisite campaign, whereas a companion paper (Briquet et al. 2012) deals with contemporaneous spectroscopy.

Located only a few degrees in the sky from V2052 Oph is

another  $\beta$  Cep star, V986 Oph (HR 6747,  $V = 6.1$ , B0III<sub>n</sub>), with an interesting history in the literature. It is among the longest-period variables ( $P \approx 0.29$  d, e.g., Jerzykiewicz 1975) of its class, and among the most luminous and hence most massive (Jones & Shobbrook 1974, Stankov & Handler 2005). It is also a rapid rotator ( $v \sin i = 300 \text{ km s}^{-1}$ , Abt, Levato & Grosso 2002) and has been classified as a single-lined spectroscopic binary ( $P_{\text{orb}} = 25.56$  d,  $e = 0.23$ , Fullerton, Bolton & Penrod 1985). Frequency analyses published by different authors indicate variability with periods between 7 to 8 hours, but all studies noted that further photometric variability is present. However, no good explanation of its physical cause could be obtained (see Cuypers, Balona & Marang (1989) for a detailed discussion). Furthermore, spectroscopic studies (Fullerton et al. 1985, Stateva, Niemczura & Iliev 2010) implied that the short period variation is due to a mode of rather high spherical degree ( $l = 4, 6$  or  $8$ ). V986 Oph was also photometrically monitored during this multisite campaign, in the hope to gain understanding of its variability.

## 2 OBSERVATIONS AND DATA REDUCTION

Our photometric observations were carried out at seven different observatories on five continents, from 11 March - 6 September 2004. An overview of the campaign observations is given in Table 1. In most cases, single-channel differential photoelectric photometry was acquired but at Sierra Nevada Observatory a simultaneous *wby* photometer was used. At observatories where no Strömgren *vy* filters were available we used Johnson *V*, with Strömgren *u* as possible complement. Finally, as the photometer at the Mercator telescope has Geneva filters installed permanently, we used this filter system. In the three seasons preceding this campaign, 72.7 hours of Geneva photometry had been obtained with the Mercator telescope. These are included here as well.

We chose two comparison stars: HR 6689 ( $V = 5.96$ , A3V) was already used as a comparison for V2052 Oph by Jerzykiewicz (1972, 1993), but was in the second paper suspected to be variable. HR 6719 ( $V = 6.34$ , B2IV) was used as a comparison star by Jerzykiewicz (1993), but also suspected of variability. Subsequent photometric studies of the star did not mention variability, but Telting et al. (2007) reported line profile variations pointing towards pulsation of high azimuthal order. Although this choice of comparison stars may not seem ideal, we did not find better suited candidates in this part of the sky. Fortunately, the comparison stars proved to be constant within the accuracy of our measurements, and did not affect our results in any way. The targets were therefore observed alternately with these comparison stars, but V986 Oph was measured only in every other cycle.

Data reduction was started by compensating for coincidence losses and subtracting sky background. Extinction corrections had to be made in two steps caused by the two comparison stars always being located at systematically different air mass (similar right ascension, but different declination and close to the celestial equator). This means that even small errors in the applied extinction coefficients cause variations in the nightly photometric zero points.

Consequently, we first determined the extinction coefficient

**Table 1.** Log of the photometric measurements of *V986 Oph* and *V2052 Oph* during the multisite campaign in 2004. Observatories are ordered according to geographical longitude.

Observatory	Telescope	Amount of data		Filter(s)	Observer(s)
		Nights	hours		
Tübitak National Observatory, Turkey	0.5m	2	6.1	V	TS
South African Astronomical Observatory	0.5m	13	50.3	uvy	EG, BN
South African Astronomical Observatory	0.75m	7	30.5	uvy	GH
South African Astronomical Observatory	0.5m	9	35.0	uV	TT
Piszkéstető Observatory, Hungary	0.5m	3	9.2	V	DL
Sierra Nevada Observatory, Spain	0.9m	4	19.7	uvby	ER
Roque de los Muchachos Observatory, Spain	1.2m Mercator	49	155.2	Geneva	KU, MB, HW, GR, AM, CB, BV
Fairborn Observatory, USA	0.75m APT	55	198.7	uvy	--
Siding Spring Observatory, Australia	0.6m	40	168.9	uvy	RRS
Total		182	673.6		

cients with the standard Bouguer method from the comparison star measurements. We then examined the differential comparison star light curves for variability, resulting in a non-detection. Next, we imposed that the average nightly photometric zeropoints for each instrumental system be the same and correspondingly amended the extinction corrections within reasonable limits. This procedure considerably improved the accuracy of our final light curves, as examined with the target star data. The residual scatter in the differential comparison star data is between 4.6 and 3.5 mmag in the Strömgren filters, and between 3.1 and 2.4 mmag in the Geneva measurements.

Consequently, we computed differential light curves of the target stars and heliocentrically corrected their timings. The single-colour measurements were binned to sampling intervals similar to that of the multicolour measurements to avoid giving them higher weight in the consequent analyses. Finally, the photometric zeropoints of the different instruments were compared between the different sites and adjusted if necessary. The resulting final combined time series, spanning 179.3 d, was subjected to frequency analysis. Light curves from the central part of our campaign are shown in Fig. 1, together with fits to be derived and commented on in what follows.

### 3 FREQUENCY ANALYSIS

The heliocentrically corrected data were searched for periodicities using the program `Period04` (Lenz & Breger 2005). This package applies single-frequency power spectrum analysis and simultaneous multi-frequency sine-wave fitting. It also includes advanced options such as the calculation of optimal light-curve fits for multiperiodic signals including harmonic and combination frequencies.

For purposes of frequency detection, the Strömgren *u* and Geneva *U* filter data were merged after checking that the oscillation amplitudes were the same within the errors. Measurements in the Strömgren *y* and Johnson and Geneva *V* filters were treated as equivalent due to the same effective wavelength of these filters, and were analysed together. After signals were believed to be detected, their presence was checked in the data of the individual filters (that is, the seven Geneva filters, Strömgren *uv*, and the combined

Strömgren *y*/Johnson *V* light curves). The Strömgren *b* filter measurements were not used because too few data are available.

Amplitude spectra were computed, compared with the spectral window functions, and the frequencies of the intrinsic and statistically significant peaks in the Fourier spectra were determined. Multifrequency fits with all detected signals were calculated step by step, the corresponding frequencies, amplitudes and phases were optimized and subtracted from the data before computing residual amplitude spectra, which were then examined in the same way.

We consider an independent peak statistically significant if it exceeds an amplitude signal-to-noise ratio of 4 in the periodogram; combination signals must satisfy  $S/N > 3.5$  to be regarded as significant (see Breger et al. 1993, 1999). The noise level was calculated as the average amplitude in a  $5 \text{ d}^{-1}$  interval centred on the frequency of interest.

For the detection of pulsation frequencies we did not make use of the pre-campaign Geneva measurements as those were carried out without using comparison stars. They therefore have about a factor of 2.5 higher scatter than the campaign data and increase the noise level in a joint analysis. However, the pre-campaign measurements could in some cases be used to derive more precise frequency values.

#### 3.1 V2052 Oph

We started by computing the Fourier spectral window of the data, which turned out reasonably clean. The strongest aliases in the *u/U* and *y/V* data have only 36% of the amplitude of the true signal. The amplitude spectrum of the data itself, dominated by the known radial mode frequency, is shown in the upper panel of Fig. 2. We chose to use the *u/U* data for presentation purposes for the pragmatical reason that all signals to be reported are detected in this data set alone.

Prewhitening the strongest signal from the data and examining the residual amplitude spectrum, we recover the stellar rotation frequency (second panel of Fig. 2). Further analysis reveals two more signals in the frequency domain of the radial mode, as well as the first harmonic of the first mode and of the rotation frequency. The residual amplitude spectrum after prewhitening these six frequencies shows a

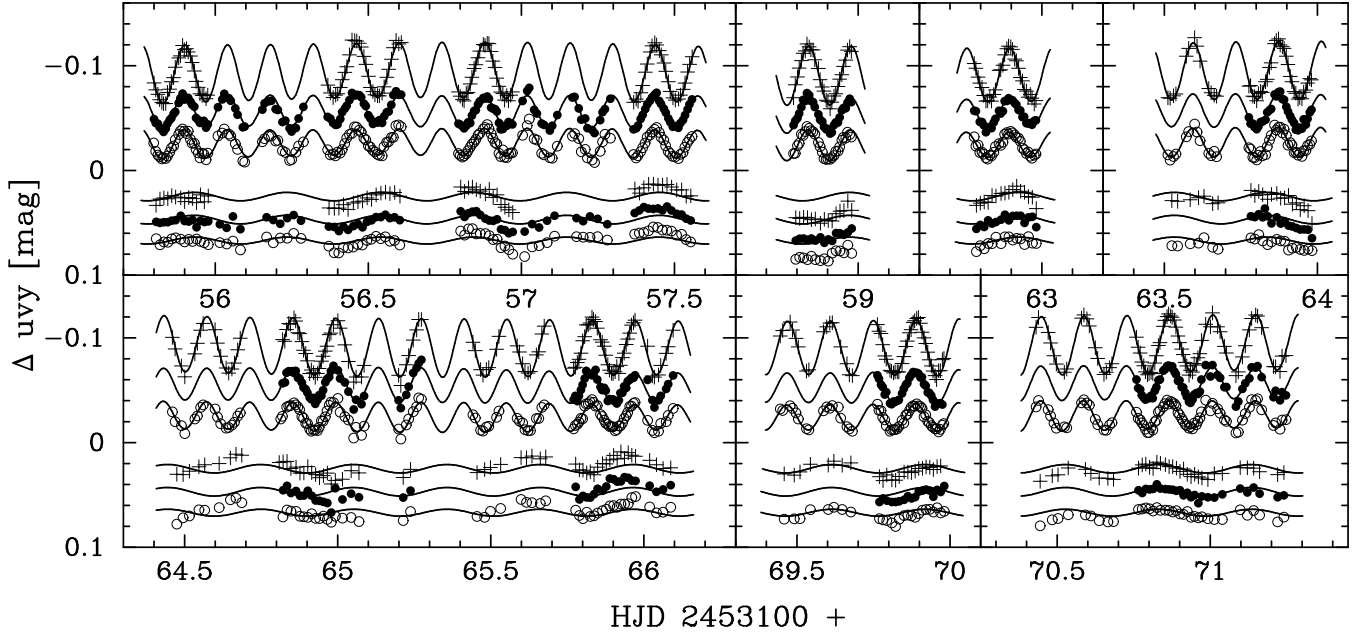


**Figure 1.** Some of our time-series photometry of V2052 Oph (upper three curves) and V986 Oph (lower three curves). The plus signs represent  $U$  or  $u$  measurements, the filled circles are  $v$  data and the open circles data in the  $V$  or  $y$  filter. The lines are the multifrequency fits derived from periodicity search.

slight  $1/f$  component, as expected from residual atmospheric effects in the data, and no signal in excess of 0.5 mmag.

With frequency solutions for the individual filters as starting values, we attempted to improve the accuracy of our frequency determinations by including the pre-campaign observations, therefore increasing the time base of the data set by a factor of 6.5. By examining the  $u/U$  and  $y/V$  data as well as confronting the results, we obtained more accurate values for all frequencies, with the exception of the second pulsation frequency where we encountered an aliasing problem. Tests on which value would result in lower residuals etc. did not allow to determine a preferred value, and the choice of this frequency did not affect the outcome on the others. We therefore adopted the average of the two candidate values, and used half the alias spacing as its uncertainty. The final values of the frequencies were then fitted to the campaign data alone but kept fixed, and only the amplitudes, phases and zeropoint were left as free parameters. The result of this procedure is listed in Table 2.

The multifrequency fit listed in the table represents the data within rms residuals between 3.4 to 2.7 mmag (Strömgren data) and between 2.6 to 2.2 mmag (Geneva data). To search for possible additional signals, we merged the residual data from all filters and computed the combined amplitude spectrum (lowest panel of Fig. 2). It contains no peak in excess of 0.35 mmag, and none with  $S/N \geq 3.2$ .

Examining the wavelength dependence of the phases of the independent signals, we noticed that the dominant pulsation signal is not in phase in all filters, as demonstrated in Fig. 3. In particular,  $\phi_v - \phi_y = 0.9 \pm 0.3^\circ$  and  $\phi_u - \phi_y = 4.2 \pm 0.2^\circ$ , i.e. the shorter the wavelength, the later light maximum/minimum is reached. As the amplitudes of the other two signals in this frequency range are by at least a factor of 15 smaller, the errors in the phases are correspondingly larger. Consequently, no statistically signif-

icant phase shifts within the different filter passbands have been detected for  $f_2$  and  $f_3$ .

The Fourier parameters of the rotational light variation change substantially from filter to filter (cf. Table 2). To determine its shape we first removed the pulsational variability from the data, and then phased them with respect to the rotation period. The Geneva data were summed into 20 phase bins and the more numerous Strömgren measurements in 25 bins. The rotational light curves are shown in Fig. 4. Unfortunately, these cannot be compared with counterparts from satellite missions such as Kepler and CoRoT as our passbands are not sufficiently red sensitive.

While we have arbitrarily phased these light curves and fits relative to HJD 2453000.000, the hatched area in Fig. 4 indicates the phase of minimum equivalent width of the ultraviolet spectral lines studied by Neiner et al. (2003). We will return to discuss this phasing in Sect. 5.1.

### 3.2 V986 Oph

The frequency analysis of our photometry of V986 Oph was performed in a similar way to that of V2052 Oph, and we also choose the  $u/U$  data for presentation. The amplitude spectrum of V986 Oph appears simple, with only one significant frequency present (Fig. 5). However, the residuals left behind a single-frequency solution are between 6.3 and 7.2 mmag per point in the Strömgren data, and between 7.0 and 8.1 mmag per point in the Geneva data, thus about a factor of two to three higher than those for V2052 Oph or for the differential comparison star data. The poorer fit for V986 Oph is also readily visible in Fig. 1. The noise level in the residual amplitude spectrum of V986 Oph is even about a factor of five higher because of the smaller amount of data points available. Furthermore, the single frequency is not significantly detected in the Geneva data alone, neither in those

**Table 2.** Multifrequency solution for our time-resolved photometry of V2052 Oph. Error estimates for the independent frequencies were derived from considering both formal errors (following Montgomery & O’Donoghue 1999) and differences in the  $u/U$  and  $y/V$  results. The quoted errors on the amplitudes are the formal values. The S/N ratio is for the  $u$  filter data.

ID	$f_1$	$f_2$	$f_3$	$2f_1$	$f_{rot}$	$2f_{rot}$
Frequency ( $d^{-1}$ )	$7.148474 \pm 0.000005$	$7.7567 \pm 0.0007$	$6.82216 \pm 0.00005$	14.296948	$0.27480 \pm 0.00002$	0.54960
$u$ Ampl. (mmag)	$26.98 \pm 0.10$	$0.84 \pm 0.10$	$0.54 \pm 0.10$	$0.52 \pm 0.10$	$2.76 \pm 0.10$	$0.78 \pm 0.10$
$v$ Ampl. (mmag)	$15.41 \pm 0.09$	$0.85 \pm 0.09$	$0.60 \pm 0.09$	$0.20 \pm 0.09$	$1.97 \pm 0.09$	$1.05 \pm 0.09$
$y$ Ampl. (mmag)	$13.37 \pm 0.08$	$0.90 \pm 0.08$	$0.56 \pm 0.08$	$0.23 \pm 0.08$	$1.62 \pm 0.08$	$0.29 \pm 0.08$
$U$ Ampl. (mmag)	$26.65 \pm 0.16$	$0.93 \pm 0.16$	$0.97 \pm 0.16$	$0.53 \pm 0.16$	$2.89 \pm 0.16$	$0.47 \pm 0.16$
$B_1$ Ampl. (mmag)	$16.08 \pm 0.15$	$0.78 \pm 0.15$	$0.97 \pm 0.15$	$0.26 \pm 0.15$	$2.56 \pm 0.15$	$1.35 \pm 0.15$
$B$ Ampl. (mmag)	$15.19 \pm 0.15$	$0.81 \pm 0.15$	$0.75 \pm 0.15$	$0.27 \pm 0.15$	$2.21 \pm 0.15$	$0.91 \pm 0.15$
$B_2$ Ampl. (mmag)	$14.40 \pm 0.16$	$0.67 \pm 0.16$	$0.60 \pm 0.16$	$0.07 \pm 0.16$	$1.88 \pm 0.16$	$0.34 \pm 0.16$
$V_1$ Ampl. (mmag)	$13.18 \pm 0.15$	$0.90 \pm 0.15$	$0.76 \pm 0.15$	$0.38 \pm 0.15$	$1.47 \pm 0.15$	$0.29 \pm 0.15$
$V$ Ampl. (mmag)	$13.22 \pm 0.13$	$0.96 \pm 0.13$	$0.74 \pm 0.13$	$0.29 \pm 0.13$	$1.40 \pm 0.13$	$0.32 \pm 0.13$
$G$ Ampl. (mmag)	$12.83 \pm 0.16$	$1.04 \pm 0.16$	$0.60 \pm 0.16$	$0.41 \pm 0.16$	$1.56 \pm 0.16$	$0.27 \pm 0.16$
$S/N$	200.2	6.4	4.0	3.9	14.1	4.0

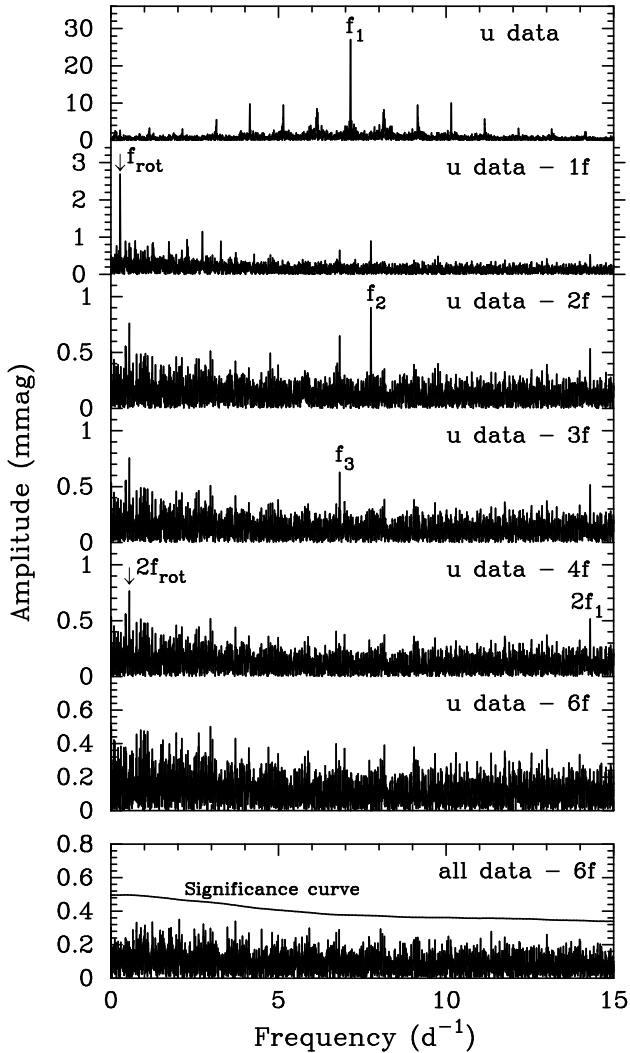


**Figure 2.** Amplitude spectra of our combined  $u/U$  filter data of V2052 Oph with consecutive prewhitening steps. The uppermost panel is practically identical with the spectral window of the data. The lowest panel shows the amplitude spectrum of the combined residuals in all filters.

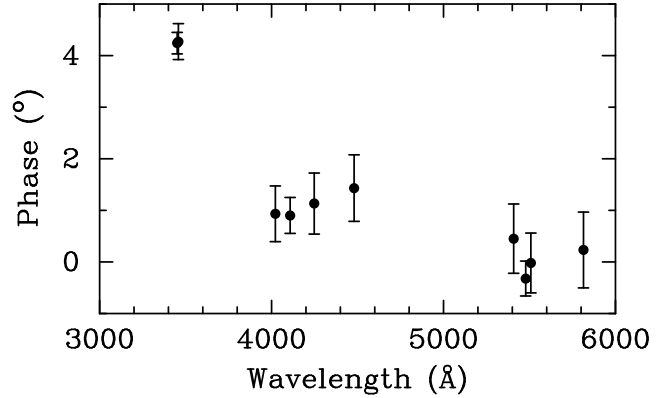


**Figure 3.** Phase of the dominant oscillation mode of V2052 Oph with respect to that in the Strömgren  $y$  filter. The dots with the error bars are the measured phase shifts in all Geneva and Strömgren filters.

obtained during the campaign, nor in the pre-campaign observations.

Investigating the matter deeper and keeping in mind that spectroscopic binarity of V986 Oph has been reported, we first looked for a possible light time effect. We therefore merged the  $u/U$ ,  $v$  and  $y/V$  data into bins no larger than 2.5 d as a compromise between not undersampling the reported 25.56 d orbit and having enough data points to determine the phase of the main light variation. We did not find a statistically significant light time effect, within a limit of 1270 s at the orbital period. In one night of observation (around HJD 2453158.9, see Fig. 1) a  $\sim 0.02$  mag drop in light, suspicious of an eclipse, was present, but another data set obtained one prospective orbital period later did not show such a feature.

Looking at the pulsation amplitude now, it appears that it dropped somewhat during the course of the campaign, but not exceeding the  $2\sigma$  level. We therefore assumed a constant amplitude for the remainder of this work, calculated the frequency of the single significant signal as a S/N-weighted average in the different Strömgren filters, and determined its

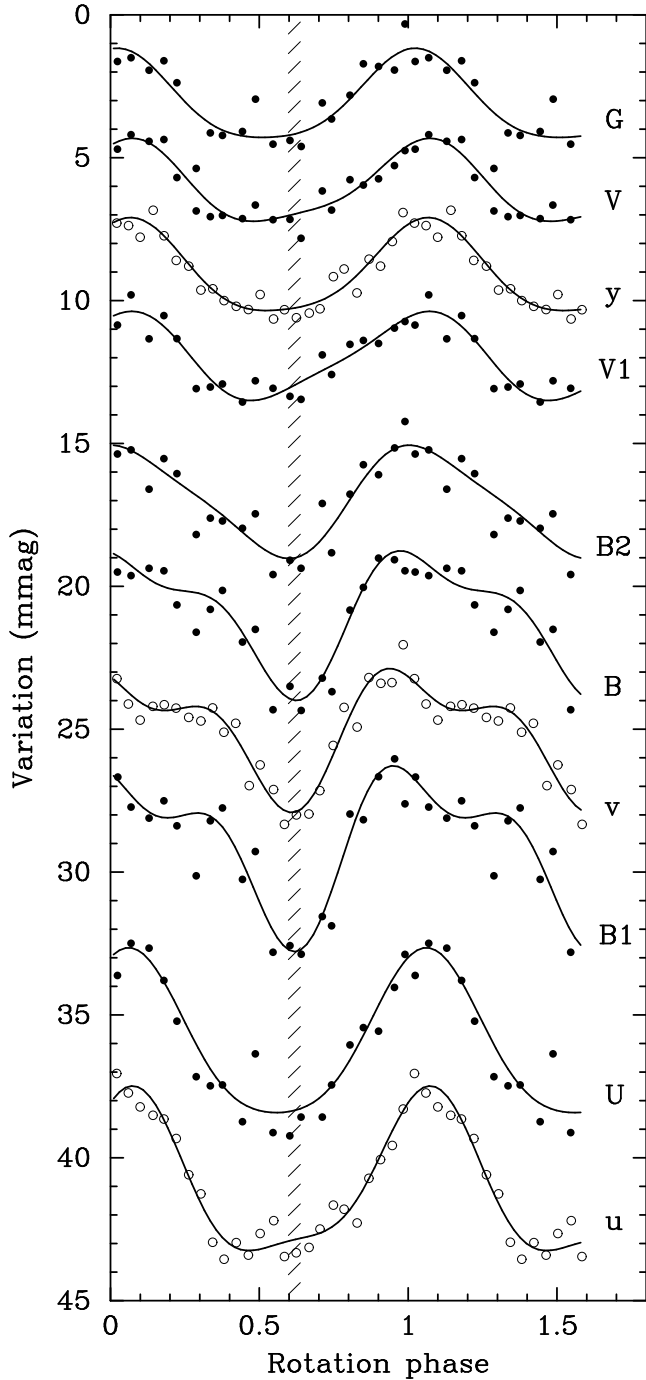


**Figure 4.** Phase diagrams of the rotational light variations of V2052 Oph in the different filters, plotted according to decreasing effective wavelength from top to bottom. Strömgen data are shown as open circles, Geneva data as filled circles, and fits are overlaid to guide the eye. The hatched area denotes the rotational phase zero as defined by Neiner et al. (2003).

amplitude and phase in all filters (see Table 3). The signal was found to be in phase within the errors in all passbands.

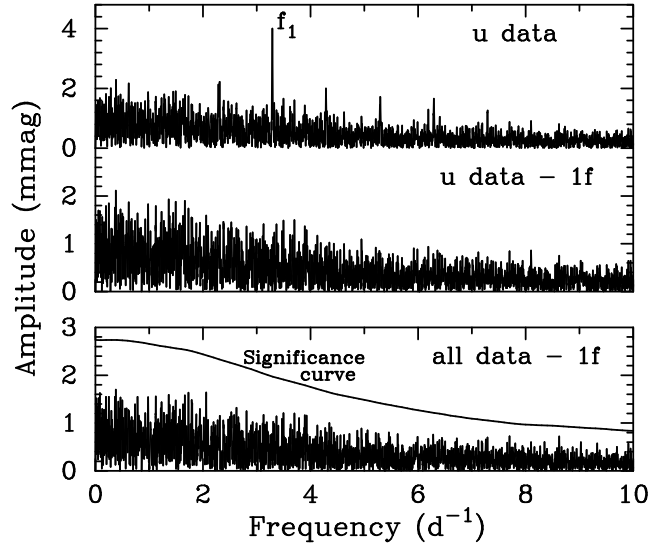


**Figure 5.** Amplitude spectra and prewhitening of our combined  $u/U$  filter data of V986 Oph.

**Table 3.** Frequency solution for our time-resolved Strömgen photometry of V986 Oph. The error on the frequency was determined from considering both formal errors (following Montgomery & O’Donoghue 1999) and differences between the  $u$ ,  $v$ , and  $y$  frequency solutions. The quoted errors on the amplitudes are the formal values. The S/N ratio is for the  $u$  filter data.

ID	$f_1$
Frequency ( $\text{d}^{-1}$ )	$3.2886 \pm 0.0003$
$u$ Ampl. (mmag)	$4.0 \pm 0.3$
$v$ Ampl. (mmag)	$4.1 \pm 0.3$
$y$ Ampl. (mmag)	$3.3 \pm 0.2$
S/N	7.1

## 4 MODE IDENTIFICATION

We now attempt to identify the spherical degree  $l$  of the pulsation modes by means of the  $uwy$  and Geneva passband amplitudes of the pulsational signals detected in the light curves. These amplitudes are to be compared with theoretically predicted ones from model computations, requiring the model parameter space to be constrained first. In other words, we need to determine the positions of the two target stars in the HR diagram as a starting point.

### 4.1 V2052 Oph

The latest spectroscopic  $T_{\text{eff}}/\log g$  values for V2052 Oph originate from Morel et al. (2006):  $T_{\text{eff}} = 23000 \pm 1000$  K and  $\log g = 4.0 \pm 0.2$ , who also list  $v \sin i = 61 \text{ km s}^{-1}$  (including the macroturbulence velocity). Niemczura & Daszyńska-Daszkiewicz (2005) derived  $T_{\text{eff}} = 23300 \pm 700$  K and  $\log g = 3.89$  from low-resolution ultraviolet spectra.

The online version of The General Catalogue of Photometric Data (GCPD; Mermilliod, Mermilliod & Hauck 1997) contains standard Strömgen and Geneva photometric colours for the star. The Strömgen system calibration by Napiwotzki, Schönberner & Wenske (1993), yields

$T_{\text{eff}} = 22700 \pm 900$  K,  $\log g = 3.9 \pm 0.3$ , and also provides an absolute magnitude estimate using the calibration of Balona & Shobbrook (1974):  $M_v = -2.59$ . The model atmosphere calibration of the Geneva system (Künzli et al. 1997) gives  $T_{\text{eff}} = 22800 \pm 500$  K,  $\log g = 3.8 \pm 0.3$ . A relatively accurate HIPPARCOS parallax (van Leeuwen 2007) is also available:  $\pi = 2.40 \pm 0.41$  mas. Adopting  $E(b - y) = 0.230$  from Strömgren photometry, this leads to  $M_v = -3.3_{-0.3}^{+0.4}$ .

All these individual determinations are in very good agreement. We therefore assume  $T_{\text{eff}} = 22900 \pm 1000$  K and  $\log g = 4.0 \pm 0.2$ . The tables by Flower (1997) then provide  $BC = -2.20$ . A comparison of the  $T_{\text{eff}}/\log g$  values with model evolutionary tracks prefers the lower value of our two absolute magnitude estimates, and suggests  $M = 9.2_{-0.7}^{+0.9} M_{\odot}$ .

Therefore we computed theoretical photometric amplitudes of the  $0 \leq l \leq 7$  modes for models with masses between 8.5 and 10.0  $M_{\odot}$  in steps of 0.5  $M_{\odot}$ , in a temperature range of  $4.340 \leq \log T_{\text{eff}} \leq 4.379$ . We used OP opacities (e.g., Seaton 2005) and the Asplund et al. (2004) mixture. An overall metal abundance  $Z = 0.012$  and a hydrogen abundance of  $X = 0.7$  has been adopted, and no convective core overshooting was used. We are aware that Morel et al. (2006) and Niemczura & Daszyńska-Daszkiewicz (2005) derived a somewhat lower metallicity, but this small inconsistency is not crucial in the mode identification process.

We extracted theoretically calculated nonadiabatic parameters from the models to determine the amplitudes in the different wavebands. This approach follows that by Balona & Evers (1999) and uses the same software, hence we refer to this paper for details on the procedure. Consequently, we computed the ratios of the theoretical amplitudes with respect to those in the Strömgren  $u$  filter, for modes of spherical degree  $0 \leq l \leq 7$  and frequencies between 6.3 and 8.3  $\text{d}^{-1}$ , and compared them with the observations (left-hand side panels of Fig. 6).

The right-hand side of Fig. 6 shows a  $\chi^2$  analysis of the photometric amplitudes, as outlined by Handler, Shobbrook & Mokgwetsi (2005). These  $\chi^2$  values use the measurements and standard errors of the amplitudes normalized to the mean of all passbands only, as the pulsation phases carry no additional information on the mode type in our case.

Because of the high  $S/N$  of the dominant mode of V2052 Oph, the amplitude ratios in all the individual Strömgren and Geneva filters could be incorporated. Such an approach is not optimal for the two low-amplitude pulsation modes. For their identification, we considered the combined  $u/U$ ,  $y/V$  as well as the Strömgren  $v$  data only.

Like all previous authors, we identify the strongest mode as radial. The theoretically predicted amplitude ratios with respect to  $u$  are systematically higher than observed. We do not believe that this is a normalisation error because the measured  $u$  and  $U$  amplitudes agree quite well. We rather think that this is due to an imperfect choice of model parameters and because we ignored the chemical peculiarity of the atmosphere. Nevertheless, the data strongly suggest that the dominant mode is radial.

The photometric amplitudes of the two other modes indicate they are of rather high and even spherical degree, most likely  $l = 4$  or 6. Our neglect of convective core overshoot does not affect these mode identifications. Whereas overshooting would modify the deeper interior structure of

the star, the photometric amplitude ratios are mostly determined in the stellar photosphere.

Neiner et al. (2003) identified the 6.822  $\text{d}^{-1}$  mode as either  $l = 3$  or 4. Therefore, the combined evidence points towards an  $l = 4$  mode, which is also the more likely identification for the 7.757  $\text{d}^{-1}$  signal because of reasons of geometrical cancellation (Daszyńska-Daszkiewicz et al. 2002). This result is supported by Briquet et al. (2012), who could spectroscopically constrain the azimuthal order of the modes and who also discuss V2052 Oph more deeply in terms of convective core overshooting.

## 4.2 V986 Oph

For this star, no spectroscopic temperature and surface gravity determinations are available in the literature. The GCPD contains Strömgren colour indices for V986 Oph, but no Geneva indices. However, we have our own photometry in this system available. In Table 4, we first compare the standard Geneva colours for V2052 Oph from the GCPD to those obtained from our data, demonstrating that they agree within a few millimagnitudes. Consequently, we trust the values that we obtained for V986 Oph.

Using the standard values in the two photometric systems as input for photometric calibrations, we must proceed with caution. First, the Geneva colours of the star are somewhat out of the range of the calibrations by Künzli et al. (1997). Extrapolating their grids, one arrives at  $T_{\text{eff}} \approx 36000$  K,  $\log g \approx 3.8$ . Second, the mean Strömgren colours listed in the GCPD and the calibrations implemented by Napiwotzki et al. (1993) yield  $T_{\text{eff}} \approx 35600$  K,  $\log g \approx 3.0$ . The latter values however imply a stellar mass in excess of  $40M_{\odot}$ , inconsistent with its B0III<sub>n</sub> spectral type. More reliable seems to be the  $T_{\text{eff}} \approx 34700$  K value from the calibration of the  $[u - b]$  index by Napiwotzki et al. (1993).

Daszyńska-Daszkiewicz (2001) determined  $T_{\text{eff}} = 30100 \pm 2300$  K,  $\log g = 4.0 \pm 0.5$ ,  $[m/H] = 0.0$ , and  $E(B - V) = 0.228 \pm 0.029$  from IUE and visual fluxes. The value for reddening is consistent with  $E(b - y) = 0.203$  from Strömgren photometry, but the effective temperature is much lower, and the surface gravity higher than from the photometric calibrations. These parameters rather imply a  $16M_{\odot}$  star, but the large error bar on  $\log g$  would allow masses up to  $25M_{\odot}$ .

For the purpose of example, we continue with  $T_{\text{eff}} = 34700 \pm 1400$  K,  $\log g = 3.8 \pm 0.3$ . We proceeded similar as we did for V2052 Oph, computing theoretical photometric amplitudes of the  $0 \leq l \leq 7$  modes, but for models with masses between 25 and 36  $M_{\odot}$  in steps of 1  $M_{\odot}$ , and in a temperature range of  $4.522 \leq \log T_{\text{eff}} \leq 4.558$ . A frequency range of 2.7 – 3.8  $\text{d}^{-1}$  was considered for nonradial modes, and 3.2 – 3.4  $\text{d}^{-1}$  for radial modes (to restrict the number of possible radial overtones). The comparison between the observed and computed amplitude ratios and a  $\chi^2$  analysis are shown in Fig. 7, where we have restricted ourselves to the Strömgren data because the oscillation was not present at a significant level in the Geneva measurements.

The results of this process clearly argue against a radial pulsation mode. Considering nonradial modes, the observed amplitude ratios imply that the dominant signal in the light curve is most likely due to an  $l = 3, 5$  or 7 mode. The lowest  $\chi^2$ , but also the smallest geometrical cancella-

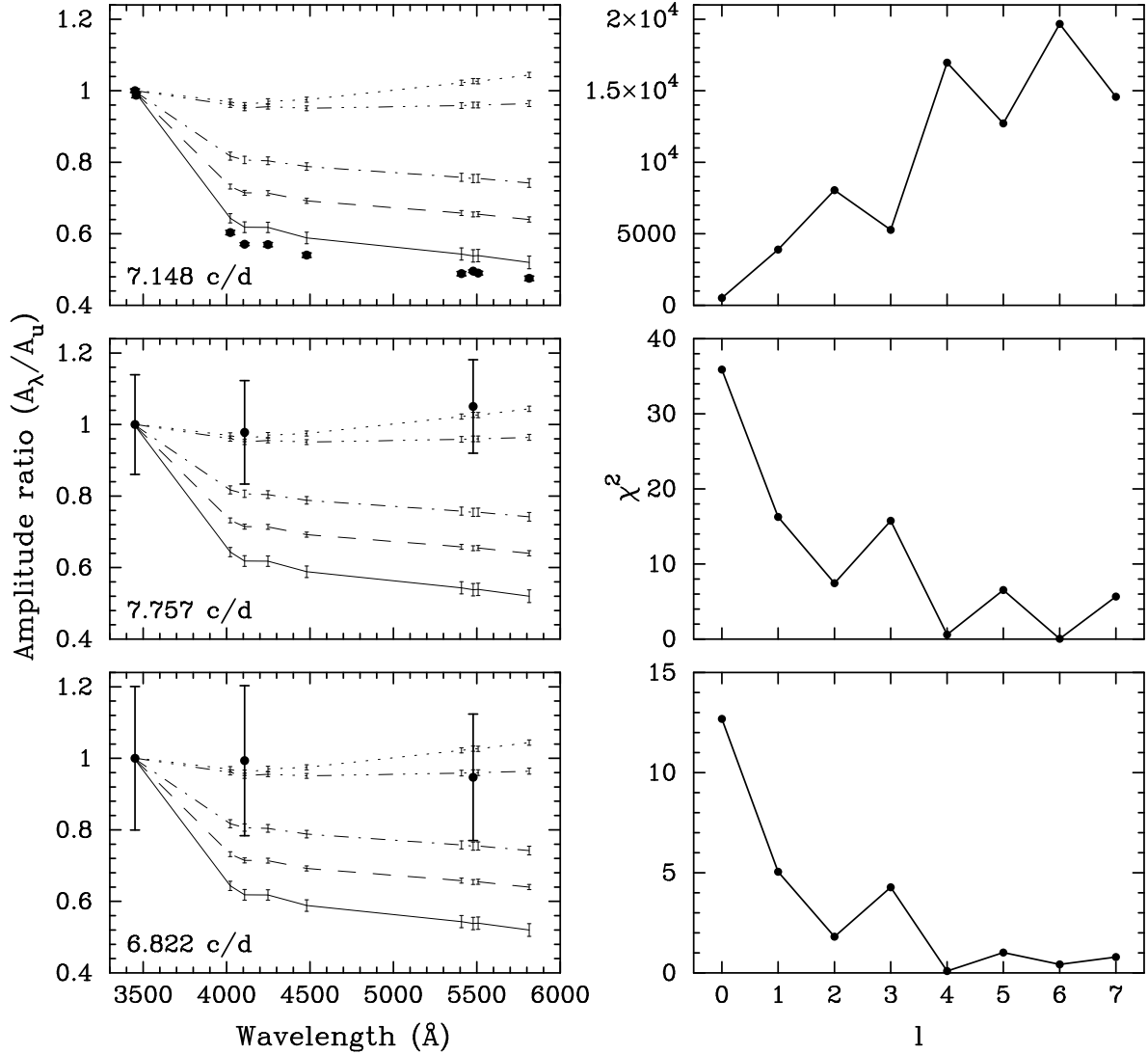


**Figure 6.** Mode identifications for V2052 Oph from a comparison of observed and theoretical amplitudes in the Strömgen and Geneva bands. Left panels: amplitude ratios, normalised to unity at  $u$ . The filled circles with error bars are the observed amplitude ratios, the thin error bars denote the uncertainties in the theoretical amplitude ratios. The full lines are theoretical predictions for radial modes, the dashed lines for dipole modes, the dashed-dotted lines for quadrupole modes, the dashed-triple-dotted lines are for  $l = 4$ , and the dotted lines for  $l = 6$  modes. The theoretical amplitude ratios for  $l = 3, 5$  and  $7$  are not shown to avoid overcrowding. Right panels:  $\chi^2$  analysis of the photometric amplitudes. The smaller  $\chi^2$ , the more likely an identification is.

tion, then favour an identification as  $l = 3$ , if taken at face value. Adopting a lower mass, as implied by the  $T_{\text{eff}}/\log g$  values by Daszyńska-Daszkiewicz (2001) results in a qualitatively consistent picture with  $l = 3, 5$  or  $7$  as the modes best reproducing the observed amplitude ratios. We refer to the discussion of the credibility of this mode identification near the end of Sect. 5.2.

## 5 DISCUSSION

### 5.1 V2052 Oph

As mentioned in the Introduction, the presence of a radial mode in the star’s pulsation spectrum allows to derive its mean density, provided the radial overtone is known. To

this end, model evolutionary tracks were computed with the Warsaw-New Jersey stellar evolution code, for a rotational velocity of  $80 \text{ km s}^{-1}$  on the ZAMS (to match the rotation period) and other input parameters as specified in Sect. 4.1. Nonadiabatic mode frequencies were calculated with the Warsaw pulsation code (e.g., see Pamyatnykh et al. (1998) for a description of these codes), and models sought that had a radial mode at the observed frequency. Fig. 8 shows the result of this procedure in the form of a theoretical HR diagram.

The effective temperature and luminosity derived for V2052 Oph in Sect. 4.1 is in best agreement with the hypothesis that the radial mode is the fundamental, but it cannot be excluded that it is the first overtone. In the first case, the stellar radius would be  $5.3 \pm 0.1 R_\odot$  and the inclination of the rotation axis thus  $54^\circ < i < 58^\circ$ , given



**Table 4.** Geneva visual magnitudes and colours<sup>1</sup> for our target stars.

Star	$VM$	$U$	$V$	$B1$	$B2$	$V1$	$G$
V2052 Oph (literature)	5.803	0.598	0.855	0.834	1.543	1.563	2.018
V2052 Oph (this work)	5.805	0.594	0.856	0.832	1.543	1.561	2.014
V986 Oph (this work)	6.119	0.268	0.984	0.791	1.584	1.682	2.163

<sup>1</sup> $VM$  is the visual magnitude, whereas the other parameters are colour indices with respect to the  $B$  band magnitude (Golay 1972).

the star’s rotation period and  $v \sin i$ . These values change to  $6.45 \pm 0.15 R_{\odot}$  and  $42^{\circ} < i < 44^{\circ}$  if the radial mode was the first overtone. Unfortunately, the scarcity of additional pulsation modes and their unknown azimuthal order leave meager prospects for asteroseismic constraints other than deriving the mean stellar density.

Attempting to fit the  $l = 4$  mode frequencies with models of the same radial mode period but varying mass gave a number of possible solutions. Unsurprisingly, if the radial mode was the fundamental, models of lower mass appear more likely because these are more evolved (cf. Fig. 8) and therefore have more mixed modes of  $l = 4$ . If the radial mode was assumed to be the first overtone, no such preference was seen.

The only statement we can make is that the two  $l = 4$  modes are unlikely to be rotationally split  $m$ -modes of the same radial overtone unless allowing for differential interior rotation. The same conclusion was reached by Briquet et al. (2012), with their independent model approach and identifications of  $m$ . The reason for this finding is that the effect of the Coriolis and centrifugal forces on the rotational frequency splitting are very similar at the given rotation rate and for  $l = 4$ , no matter whether the mode under consideration is a  $p$ ,  $g$  or mixed mode.

Neiner et al. (2003) determined a very precise rotation period for the star despite a non-optimal temporal distribution of their data in terms of annual aliasing problems. The rotation period we have obtained is consistent within the errors with the more precise one by Neiner et al. (2003), and accurate enough to rule out that their value is affected by aliases. Therefore we confirm 3.638833 d as the best available rotation period of V2052 Oph.

In Fig. 4, the phase of minimum rotational light variation coincides with minimum magnetic field strength and minimum UV spectral line equivalent width, as determined by Neiner et al. (2012a). In  $B1, v$  and  $B$  there is also a double maximum, as in the UV line strength. The shape of these variations indicates that both magnetic poles are seen during a rotation cycle, i.e. the sum of the angles of the inclination of the rotation axis and the magnetic obliquity  $i + \beta$  must exceed  $90^{\circ}$ .

Neiner et al. (2012a) determined  $i$  to be  $53^{\circ} < i < 77^{\circ}$  from modelling Stokes profiles. This is consistent with the inclination of the rotation axis we obtained with a stellar radius corresponding to radial fundamental mode pulsation, but not with the value assuming the radial mode is the first overtone. We therefore rule out the latter possibility. Using  $r = B_{\min}/B_{\max} = \cos(i - \beta)/\cos(i + \beta)$ , where  $r$  is the ratio of the minimum and maximum magnetic field strength of

the rotation cycle, and the  $r$  values determined by Neiner et al. (2012a), we obtain  $58^{\circ} < \beta < 66^{\circ}$ .

As mentioned, the light curve of V2052 Oph shows rotational modulation (Fig. 4) in phase with the magnetic field and UV wind variations. This could be due to spots at the surface of the star (such as those suggested by Neiner et al. 2012a) or magnetically confined clouds in the circumstellar environment (e.g. Townsend & Owocki 2005). Using the magnetic field value ( $B_{\text{pol}} = 400$  G, Neiner et al. 2012a), the wind velocity estimated in UV data ( $v_{\text{inf}} = 500 \text{ km s}^{-1}$ , Neiner et al. 2003), the stellar parameters from Sect. 4.1 and above ( $M = 9.2 M_{\odot}$ ,  $R = 5.3 R_{\odot}$ ,  $v \sin i = 61 \text{ km s}^{-1}$ ,  $i = 56^{\circ}$ ), and a mass loss typical of a B2 star ( $\dot{M} = 10^{-9} M_{\odot} \text{ yr}^{-1}$ ), we derived the magnetic confinement parameter  $\eta_*$  (see ud-Doula & Owocki 2002) of V2052 Oph.

We obtained that  $\eta_* = 2576$ , the Alfvén radius is  $R_A = 7.12R$ , and the Kepler radius is  $R_K = 3.05R$ . This implies that magnetic confinement should occur ( $\eta_* > 1$ ) at the magnetic equator between  $R_K$  and  $R_A$ . Indeed in this region wind particles get trapped in closed field loops and remains centrifugally supported. Above  $R_A$  material escapes as the wind stretches field lines open. Below  $R_K$  material lacks sufficient centrifugal support and falls back onto the star, but this transient material can still create a dynamical magnetosphere (ud-Doula, Owocki & Townsend 2008, Petit et al. 2011).

However, a centrifugally supported magnetosphere usually produces  $H\alpha$  emission and such emission has never been observed in V2052 Oph. Moreover, Oskinova et al. (2011) showed that V2052 Oph is only very weakly X-ray luminous. A centrifugally supported magnetosphere could exist without producing  $H\alpha$  or much X-ray emission if the density or temperature of the wind was not appropriate or if the confinement timescale was too long (see, e.g., Neiner et al. 2012b for a more detailed discussion of the emission measure in magnetospheres).

V2052 Oph is not the only magnetic  $\beta$  Cep star known. Telting, Aerts & Mathias (1997) spectroscopically detected rotationally equally split frequencies around the dominant radial pulsation mode of  $\beta$  Cep itself, and discussed whether these could be temperature spots on the surface or due to a magnetically distorted oblique pulsation mode (the magnetic field was reported by Henrichs et al. 2000). On the other hand, no such rotational frequency splitting has been reported for  $\xi^1$  CMa (Saesen, Briquet & Aerts 2006, Fournelle-Ravard et al. 2011). Both stars have a single or dominant radial mode, such as V2052 Oph. For our target, we find no signals at frequencies split by one or two times the rotation frequency around the radial pulsation, within a limit of 0.2 mmag in amplitude.

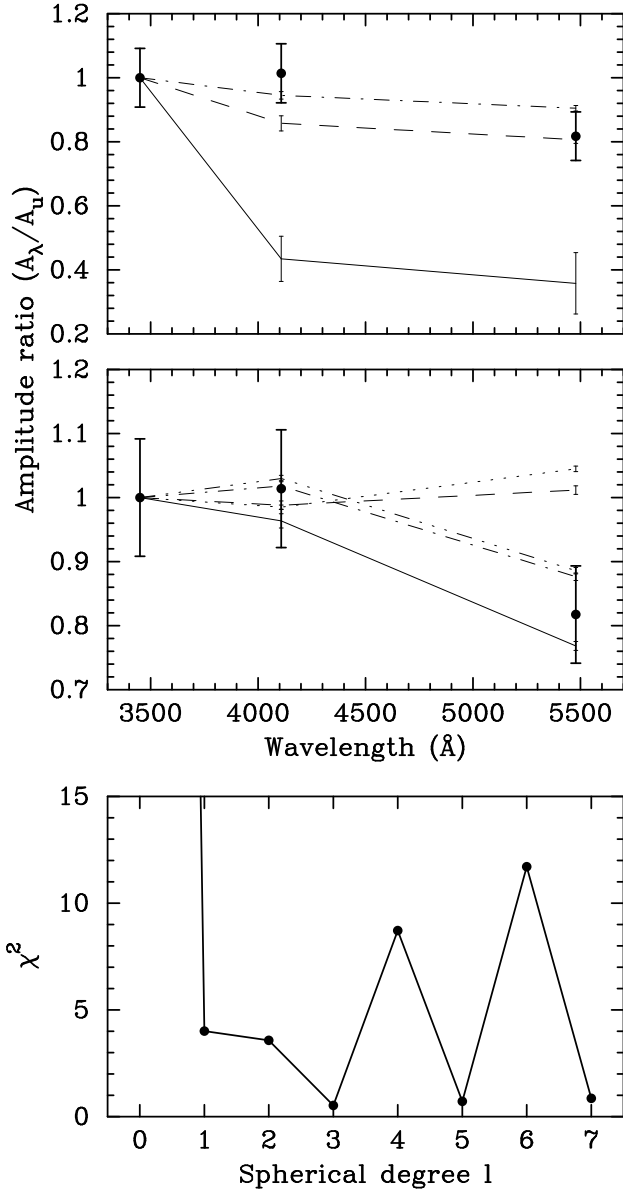


**Figure 7.** Mode identifications for V986 Oph from a comparison of observed and theoretical  $uvy$  amplitude ratios, normalised at  $u$ . In the upper two panels, the filled circles with error bars are the observed amplitude ratios. The full line in the uppermost panel is the theoretical predictions for radial modes, the dashed line for dipole modes, and the dashed-dotted lines for quadrupole modes. In the middle panel, the full line is for  $l = 3$  modes, the dashed line for  $l = 4$ , the dashed-dotted lines for  $l = 5$ , the dotted lines for  $l = 6$ , and the dashed-triple-dotted lines are for  $l = 7$  modes. The thin error bars denote the uncertainties in the theoretical amplitude ratios. The lowest panel shows the results of a  $\chi^2$  analysis of the amplitudes.

## 5.2 V986 Oph

In Sect. 3.2 we remarked that the residual scatter in our light curves prewhitened by the single coherent frequency is considerably higher than that in the other time series from this campaign. Since the two comparison stars are farther apart from each other on the sky as V986 Oph is from either of them, this cannot be due to residual data reduction er-

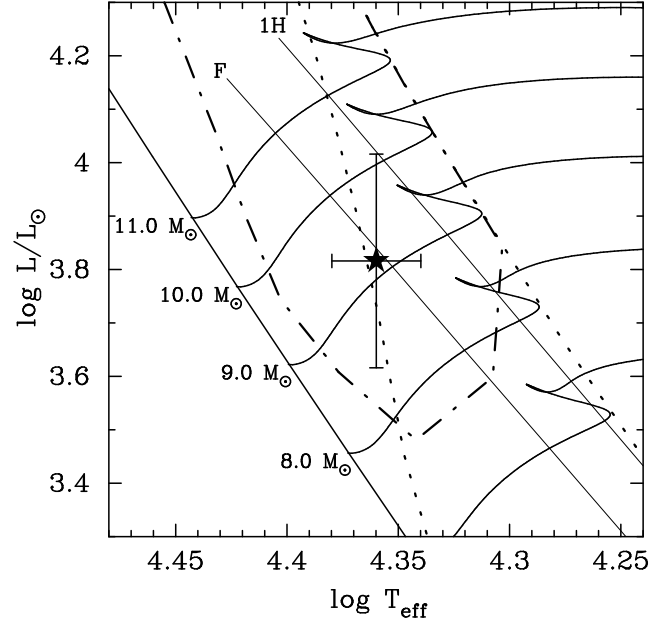


**Figure 8.** Constraints on the position of V2052 Oph (star symbol with error bars) in the HR Diagram. Some stellar evolutionary tracks are plotted and labelled with corresponding masses, and the theoretical edges of the  $\beta$  Cep (dashed-dotted line) and Slowly Pulsating B (SPB) star (dotted line) instability strips (Pamyatnykh & Ziomek 2007) are shown. The thin full lines connect models with radial modes at the observed frequency; "F" stands for the fundamental mode, "1H" for the first overtone.

rors. Furthermore, the scatter in colour light curves of V986 Oph, e.g.  $u - y$ , is much less than the residual scatter in the individual passbands, and virtually the same as in the differential comparison star data in the same filter combination. We therefore conclude that this high apparent scatter in the light curves actually represents intrinsic variability of V986 Oph, and that this kind of variability is not dominated by changes in the stellar effective temperature.

The main variability frequency we found is consistent with the one in the 1987 data by Cuypers et al. (1989), and the amplitude is comparable. However, these authors also remarked on the presence of longer-term light variations on time scales longer than half a day. We do not find coherent variability on such time scales in the complete data set. We therefore subdivided our measurements into chunks comparable to the extent of the data by Cuypers et al. (1989) and analysed the residuals after prewhitening the main periodicity. Longer-term variability is present, but we find nothing periodic. Unfortunately, our data have too low a duty cycle for invoking techniques such as Time-Fourier analysis to search for some possible short-lived periodic variations.

V986 Oph is not the first case of a  $\beta$  Cep star for which unknown additional variability besides that of pulsational origin has been found. Jerzykiewicz (1978) and Handler et al. (2006) discussed this problem for the star 12 (DD) Lac ( $11.5 M_\odot$ ), Jerzykiewicz et al. (2005) for  $\nu$  Eridani ( $9.6 M_\odot$ ), and Handler et al. (2005) for  $\theta$  Oph ( $\sim 8.5 M_\odot$ ), where it seems present at a lower level. On the other hand, for V2052 Oph we did not find such evidence, and it is hardly, if at all present in the MOST photometry of  $\gamma$  Peg ( $8.5 M_\odot$ , Handler

et al. 2009). One might therefore speculate that the more massive the star, the stronger this additional variability.

In this context it is very interesting that Blomme et al. (2011) analysed CoRoT light curves of three O stars and also found some apparently incoherent variability, in all three targets. These authors suggested that it could be due to subsurface convection, granulation or wind variability. On the other hand, Balona et al. (2011) suggested that the low frequencies observed in the amplitude spectra of Kepler B-type stars are due to many simultaneous gravity mode oscillations with high spherical degree. The present data for V986 Oph do not allow us to distinguish between those possibilities, and also not to argue against pulsation in modes of high spherical degree, because those would not generate strong colour variability (cf. Daszyńska-Daszkiewicz & Pamyatnykh 2012). However, we do point out that this presently unexplained variability may occur in stars with masses down to  $9 M_{\odot}$ .

Some authors have (e.g., Jerzykiewicz 1975) questioned the membership of V986 Oph to the class of  $\beta$  Cep stars due to its long variability period. Because the star rotates rapidly, several possibilities need to be considered. With the temperature and luminosity estimate for V986 Oph from the photometric data in Sect. 4.2 the star would have a radius of  $12 \pm 4 R_{\odot}$ , which yields a rotation period of about two days assuming  $v_{rot} = 300 \text{ km s}^{-1}$ . As the critical (break-up) rotational velocity of such massive stars is around  $400 \text{ km s}^{-1}$ , the rotation frequency cannot exceed  $0.7 \text{ d}^{-1}$ . For the possibility of a  $\sim 16 M_{\odot}$  star, this upper limit increases to  $2.7 \text{ d}^{-1}$ . Therefore we rule out that the single coherent signal we found in the light curves of V986 Oph is due to rotation.

Another hypothesis would be a g mode frequency rotationally split into the p/mixed mode domain. However, because of the large uncertainties in the stellar mass and effective temperature, we cannot reach a conclusion for this possibility and stay with the assumption that V986 Oph is a  $\beta$  Cephei star.

The frequency of the single coherent variability signal has changed from the first published observations, as summarized by Jerzykiewicz (1975). Up to his paper, the frequency was quoted as  $3.44 \text{ d}^{-1}$  or somewhat higher. Later, Fullerton et al. (1985) gave two different periods for the different seasons 1980 and 1984, the latter consistent with the  $3.29 \text{ d}^{-1}$  frequency determined by Cuypers et al. (1989) and us. Therefore this frequency must have changed some time in the 1980's, by an amount too large to be explicable by stellar evolution. Most likely, it is just due to a change of the dominant pulsation mode of the star, which has been observed in at least one other  $\beta$  Cep star before (Jerzykiewicz & Pigulski 1996).

Concerning the amplitude, the published light range is of the order of 0.02 to 0.03 mag. This is comparable to what we see in our data (cf. Fig. 1). However, the amplitude of the main periodicity may have dropped, or the larger values reported in the literature, based on much smaller data sets, are biased by the incoherent variability. Jerzykiewicz (1975) already remarked on the unusually low  $U/B$  amplitude ratio from the viewpoint of  $\beta$  Cep pulsation, as manifested in the data of Hill (1967). Our observed  $u/v$  amplitude ratio is consistent with that, and can be best explained with an odd- $l$  mode of fairly high degree ( $l \geq 3$ ).

Such a mode identification is unexpected for two rea-

sons. First, geometrical cancellation is very strong for modes with odd spherical degree larger than one (Daszyńska-Daszkiewicz et al. 2002). Second, for such a rapidly rotating star one would naively expect a preference for  $l = 2$  modes due to the distortion of the stellar shape. However, as demonstrated by Townsend (2003), our implicit assumption that the geometry of the pulsation mode of V986 Oph can be described in the form of a single spherical harmonic may not be correct. Also, the photometric amplitudes of rapidly rotating stars depend on the azimuthal order of the modes as well as the aspect under which they are viewed (Townsend 2003).

Our most likely mode identification as  $l = 3$  is therefore uncertain and calls for a high-resolution spectroscopic investigation. This would also serve to derive more reliable values of the stellar temperature and surface gravity than we have available. In particular, it would be interesting to confirm or reject the high stellar mass we inferred.

## 6 CONCLUSIONS

In an attempt to understand the pulsational behaviour of  $\beta$  Cep stars that are more complicated than those previously studied with asteroseismic methods (slow rotators with fairly large amplitudes), we have carried out an extensive multisite campaign. Results from the photometric investigation were however insufficient to perform a detailed asteroseismic study, as only three pulsation modes were detected for V2052 Oph, and one for V986 Oph.

However, it is interesting that the nonradial modes present are of higher spherical degree than commonly found. We are aware of only a few cases with observationally identified  $l = 3$  (e.g., Briquet et al. 2009) or  $l = 4$  modes (e.g., Aerts, Waelkens & De Pauw 1994), and these stars tend to rotate more rapidly than those dominated by modes of low spherical degree.

Therefore the often-made assumption that  $\beta$  Cep pulsation modes detected photometrically from the ground are  $l \leq 2$  needs to be questioned. In the context of highly sensitive space photometry this assumption is of course even more doubtful. Since the amplitude reduction due to geometrical cancellation of sufficiently high- $l$  pulsation modes only goes as  $\sim l^{-1/2}$  (e.g., Daszyńska-Daszkiewicz et al. 2002), the gain in the number of oscillation frequencies detected is offset by the larger uncertainty in mode typing.

Photometric identifications of modes with high spherical degree become largely degenerate for even and odd modes with  $l \geq 3$ . This situation can be relieved by obtaining simultaneous spectroscopy. The amplitude ratios and phase shifts between the radial velocity and light curves allow some separation between high- $l$  modes (Daszyńska-Daszkiewicz & Pamyatnykh 2012), and of course line-profile variations offer a multitude of possibilities for identifying modes (e.g., Telting 2008 and references therein).

It therefore seems that if we are to understand the interior structure of more rapidly rotating  $\beta$  Cep stars than those studied so far, all observationally and theoretically available tools need to be exploited. Photometric measurements need to be made in multiple passbands, and (simultaneous) spectroscopic observations must be acquired. The interpretation of these data may require the inclusion of the

effects of rotation on a star-to-star basis because observables can be affected to the extent that mode identifications, a prerequisite for asteroseismology, may be erroneous (see Townsend 2003). However, to shed light on important astrophysical problems, such as internal angular momentum transport, such concerted efforts will be worthwhile.

## ACKNOWLEDGEMENTS

This work has been supported by the Austrian Fonds zur Förderung der wissenschaftlichen Forschung under grant R12-N02. KU acknowledges financial support by the Spanish National Plan of R&D for 2010, project AYA2010-17803. GH thanks Jadwiga Daszyńska-Daszkiewicz and Patrick Lenz for helpful discussions, and Luis Balona for permission to use his software. EG acknowledges support from the Austrian Science Fund (FWF), project number P19962-N16. MB is a F.R.S.-FNRS Postdoctoral Researcher, Belgium.

This work is based in part on observations made with the Mercator Telescope, operated on the island of La Palma by the Flemish Community, at the Spanish Observatorio del Roque de los Muchachos of the Instituto de Astrofísica de Canarias, and at the South African Astronomical Observatory.

This paper has been typeset from a  $\text{\LaTeX}$  file prepared by the author.

## REFERENCES

- Abt H. A., Levato H., Grosso M. 2002, *ApJ* 573, 359  
Aerts C., Waelkens C., de Pauw M., 1994, *A&A* 286, 136  
Aerts C., Christensen-Dalsgaard J., Kurtz D. W. 2010, *Asteroseismology*, (Springer-Verlag, Berlin)  
Aerts C., et al. 2003, *Science*, 300, 1926  
Aerts C., Briquet M., Degroote P., Thoul A., van Hoolst T., 2011, *A&A* 534, 98  
Asplund M., Grevesse N., Sauval A. J., Allende Prieto C., Kiselman D., 2004, *A&A* 417, 751  
Balona L. A., Shobbrook R. R., 1974, *MNRAS* 211, 375  
Balona L. A., Evers E. A., 1999, *MNRAS* 302, 349  
Balona L. A., et al., 2011, *MNRAS* 413, 2403  
Blomme R., et al., 2011, *A&A* 533, A4  
Breger M., et al., 1993, *A&A* 271, 482  
Breger M., et al., 1999, *A&A* 349, 225  
Briquet M., et al., 2009, *A&A* 506, 269  
Briquet M., et al., 2012, *MNRAS*, to be submitted  
Crawford D. L., 1978, *AJ* 83, 48  
Cugier H., Dziembowski W. A., Pamyatnykh A. A., 1994, *A&A* 291, 143  
Cuyppers J., Balona L. A., Marang F. 1989, *A&AS*, 81, 151  
Daszyńska-Daszkiewicz J., 2001, PhD thesis, University of Wrocław  
Daszyńska-Daszkiewicz J., Pamyatnykh A. A., 2012, in *Impact of new instrumentation and new insights in stellar pulsations* eds. L. A. Balona et al., *Astrophys. Space Sci. Proc. series*, in press (arXiv:1112.2572)  
Daszyńska-Daszkiewicz J., Dziembowski W. A., Pamyatnykh A. A., Goupil M.-J., 2002, *A&A* 392, 151  
Desmet M., et al., 2009, *MNRAS* 396, 1460  
Flower P. J., 1996, *ApJ* 469, 355  
Fourtune-Ravard C., Wade G. A., Marcolino W. L. F., Shultz M., Grunhut J. H., Henrichs H. F., in *Active OB stars: structure, evolution, mass loss, and critical limits*, Proc. IAU Symp. 272, p. 180  
Frost E. B., 1902, *ApJ*, 15, 340  
Fullerton A. W., Bolton C. D., Penrod G. D., 1985, *JRASC* 79, 236  
Golay M., 1972, *Vistas in Astronomy* 14, 13  
Handler G., et al., 2006, *MNRAS* 365, 327  
Handler G., et al., 2009, *ApJ* 698, L56  
Handler G., in *Planets, Stars and Stellar Systems*, eds. T. D. Oswalt et al., Springer-Verlag, Berlin, 2012, in press (Chapter 27)  
Handler G., Shobbrook R. R., Mokgwetsi T., 2005, *MNRAS* 362, 612  
Hauck B., Mermilliod M., 1998, *A&A* 129, 431  
Henrichs H. F., et al., 2000, in *The Be Phenomenon in Early-Type Stars*, eds. M. A. Smith & H. F. Henrichs, ASP Conf. Ser. 214, p. 324  
Heynderickx D., Waelkens C., Smeyers P., 1994, *A&AS* 105, 447  
Hill G., 1967, *ApJS* 14, 263  
Jerzykiewicz M., 1972, *PASP* 84, 718  
Jerzykiewicz M., 1975, *Acta Astr.* 25, 81  
Jerzykiewicz M., 1978, *Acta Astr.* 28, 465  
Jerzykiewicz M., 1993, *A&AS* 97, 421  
Jerzykiewicz M., Pigulski, A., 1996, *MNRAS*, 282, 853  
Jerzykiewicz M. et al. 2005, *MNRAS* 360, 619  
Jones D. H. P., Shobbrook R. R., 1974, *MNRAS* 166, 649  
Künzli M., North P., Kurucz R. L., Nicolet B., 1997, *A&AS* 122, 51  
Ledoux P., 1951, *ApJ* 114, 373  
van Leeuwen F., 2007, *A&A* 474, 653  
Lenz P., Breger M., 2005, *Comm. Asteroseism.* 146, 53  
Mermilliod J.-C., Mermilliod M., Hauck B., 1997, *A&AS* 124, 349  
Montgomery M. H., O'Donoghue D., 1999, *Delta Scuti Star Newsletter* 13, 28 (University of Vienna)  
Morel T., Butler K., Aerts C., Neiner C., Briquet M., 2006, *A&A* 457, 651  
Napiwotzki R., Schönberner D., Wenske V., 1993, *A&A* 268, 653  
Neiner C., et al., 2003, *A&A* 411, 565  
Neiner C., et al., 2012a, *A&A* 537, A148  
Neiner C., et al., 2012b, *A&A*, in press  
Niemczura E., Daszyńska-Daszkiewicz J., 2005, *A&A* 433, 659  
Pamyatnykh A. A., Ziomek, W., 2007, *Comm. Asteroseism.* 150, 207  
Pamyatnykh A. A., Dziembowski W. A., Handler G., Pikall H., 1998, *A&A* 333, 141  
Pamyatnykh A. A., Handler G., Dziembowski W. A., 2004, *MNRAS* 350, 1022  
Petit V., et al., 2012, in *Four Decades of Massive Star Research*, ed. L. Drissen, ASP Conf. Ser., in press (arXiv:1111.1238)  
Pigulski A., Pojmański G., 2008, *A&A* 477, 917  
Saesen S., Briquet M., Aerts C., 2006, *Comm. Asteroseism.* 147, 109  
Seaton M. J., 2005, *MNRAS* 362, L1  
Stankov A., Handler G., 2005, *ApJS* 158, 193  
Stateva I., Niemczura E., Iliev I., 2010, *Pub. Astr. Obs. Belgrade* 90, 179  
Telting J. H., 2008, *Comm. Asteroseism.*, 157, 112  
Telting J. H., Aerts C., Mathias, P., 1997, *A&A* 322, 493  
Telting J. H., Schrijvers C., Ilyin I. V., Uytterhoeven K., De Ridder J., Aerts C., Henrichs H. F., 2006, *A&A* 452, 945  
Townsend R. H. D., 2003, *MNRAS* 343, 125  
Townsend R. H. D., Owocki S. P., 2005, *MNRAS* 357, 251  
ud-Doula A., Owocki S. P., 2002, *ApJ* 576, 413  
ud-Doula A., Owocki S. P., Townsend R. H. D., 2008, *MNRAS*, 385, 97